Journal of Computational and Applied Mathematics 280 (2015) 294–309

Contents lists available at ScienceDirect

Journal of Computational and Applied Mathematics

journal homepage: www.elsevier.com/locate/cam

A generalized multiscale finite element method for the Brinkman equation

Juan Galvis [a,*], Guanglian Li [b], Ke Shi [b]

[a] Departamento de Matemáticas, Universidad Nacional de Colombia, Bogotá D.C., Colombia

[b] Department of Mathematics and Institute for Scientific Computation (ISC), Texas A&M University, College Station, TX 77843-3368, USA

ARTICLE INFO

Article history:
Received 20 April 2014
Received in revised form 14 July 2014

Keywords:
Brinkman equation
Generalized multiscale finite element method
Mixed finite element

ABSTRACT

In this paper we consider the numerical upscaling of the Brinkman equation in the presence of high-contrast permeability fields. We develop and analyze a robust and efficient Generalized Multiscale Finite Element Method (GMsFEM) for the Brinkman model in two dimensions. In the fine grid, we use mixed finite element method with the velocity and pressure being continuous piecewise quadratic and piecewise constant finite element spaces, respectively. Using the GMsFEM framework we construct suitable coarse-scale spaces for the velocity and pressure that yield a robust mixed GMsFEM. We develop a novel approach to construct a coarse approximation for the velocity snapshot space and a robust small offline space for the velocity space. The stability of the mixed GMsFEM and a priori error estimates are derived. A variety of two-dimensional numerical examples are presented to illustrate the effectiveness of the algorithm.

1. Introduction

In this paper, we design and analyze an efficient numerical method based on the generalized multiscale finite element method (GMsFEM) framework for Brinkman type system of partial differential equations in the context of mixed finite element method. The Brinkman equation is widely accepted in the mathematical modeling of flows in heterogeneous fields, e.g., vuggy carbonate reservoirs, low porosity filtration devices and biomedical hydrodynamic studies [1,2]. In these applications, the simple Darcy model is only capable of modeling slow flow problems [3,4], thus Darcy flow is not suitable to cavity problems. Moreover, even though the Darcy–Stokes interface model is capable to describe the flow of a viscous fluid in cavity and porous media, it is not practically feasible since the precise information about the location and geometry of the interface between vugs and the porous matrix is inaccessible, neither are the experimentally determined values related to the interface conditions. The Brinkman flow behaves like a Darcy flow and a Stokes flow for regions with very large permeability values and with small permeability values, respectively. Hence, in comparison with the popular Stokes–Darcy interface model, the Brinkman model can describe both a Stokes and a Darcy flow without using a complex interface condition. Therefore, the accuracy and efficiency of the Brinkman flow simulation is of significant practical interest [5–8]. In our earlier work [9], we derived homogenization results for high-contrast Brinkman flow in a periodic permeability field. We showed that the homogenization method can simplify the high-contrast periodic Brinkman model, and the resulting solution is a good approximation of the original Brinkman model.

* Corresponding author.
E-mail address: jcgalvisa@unal.edu.co (J. Galvis).

http://dx.doi.org/10.1016/j.cam.2014.11.038
0377-0427/

In this work, we investigate the high-contrast Brinkman flow in general high-contrast permeability fields instead of the periodic fields as analyzed in [9]. In most porous media related flow problems, there always exists a coefficient that can vary several orders of magnitude within the analysis domain. This type of media is usually referred as a high-contrast medium. Often, model reduction techniques are required for efficiently resolving such multiscale problems. These techniques all rely on a coarse grid approximation, obtained by discretizing the problem on a coarse grid, much coarser than the fine grid, and a suitable coarse-grid formulation of the problem. In the literature, several different approaches have been proposed to obtain the coarse-grid formulation, which can be roughly divided into upscaling models [10,11] and multiscale methods (see, e.g., [12–18] and the references therein). Among existing multiscale methods, the GMsFEM framework [15,19] of recent origin has demonstrated great promise; see [15,20–22,18,23,19] for methodological developments and extensive applications. In the GMsFEM, the coarse grid problem is obtained by locally constructing reduced order models for the solution space on coarse regions and then employing a global formulation on the resulting reduced space.

The Brinkman model can be written as

$$\begin{aligned} &\nabla p - \mu \Delta u + \kappa^{-1} u = f \quad \text{in } \Omega, \\ &\operatorname{div} u = 0 \quad \text{in } \Omega, \end{aligned}$$

where p is the fluid pressure, u represents the velocity, f denotes the forcing term and $\Omega \in R^n$, $n = 2, 3$ with polyhedral boundary. Here, μ is the viscosity and $\kappa = \kappa(x)$ is a heterogeneous multiscale coefficient that models the permeability of the porous medium. We assume that the variations of κ occur within a very fine scale and therefore a direct simulation of this model is costly.

As mentioned above, one of the main advantages of the Brinkman model is that it can capture Stokes and Darcy type flow behavior depending on the value of κ without the usage of a complex interface condition as needed in the Stokes–Darcy interface model. This is very convenient when modeling complicated porous scenarios such as a vuggy medium. However, this advantage of the Brinkman model does not come for free: it brings the challenge of effectively designing numerical homogenization or upscaling methodologies since the resulting upscaling method must capture the correct flow behavior in corresponding regions. This difficulty increases in the case of high-contrast coefficients due to the fact that, in a single coarse region, the permeability field can have variations of several order of magnitude that make it difficult to compute effective parameters for the permeability or boundary conditions using classical multiscale finite element methods.

In this work, we develop an efficient (multiscale) solver based on the GMsFEM framework [19] for the Brinkman flow in heterogeneous high-contrast permeability fields. As far as we know, there has not been any paper on the GMsFEM of Brinkman flow in high-contrast flow. GMsFEM is based on MsFEM, and it is an enrichment of MsFEM in the sense that it adds more basis in each coarse neighborhood to approximate the high-contrast problem more accurately. Upscaling approaches are another type of model reduction method derived from homogenization. In this framework, as in many other multiscale model reduction techniques, one divides the computation into two stages, i.e., the offline stage and the online stage. In the offline stage, a reduced dimension space is constructed, and it is then used in the online stage to construct multiscale basis functions. These multiscale basis functions can be re-used for any input parameter to solve the problem on a coarse grid. The main idea behind the construction of the offline and online spaces is to design appropriate local spectral-based selection of important modes that generate the snapshot space. In [19], several general strategies for designing the local spectrum-based selection procedures were proposed. Here, we focus on the generation of snapshots spaces, and rigorous convergence analysis of the resulting coarse approximation. Further, we establish stability estimate of the mixed GMsFEM (in the form of inf–sup conditions) for the proposed reduced dimension spaces. The convergence analysis extends that for elliptic equations with high-contrast coefficients [15].

We present four numerical examples to illustrate the performance of the proposed approach. One challenge with the Brinkman model is the construction of a stable finite element discretization, and lots of researchers are working on it [8,24]. In this paper, we apply the simple $Q2\backslash Q0$ element for the sake of simplicity since the focus of our work is on the stability of the GMsFEM for Brinkman flow. We study the model with different high-contrast parameter κ^{-1}. As we know that the velocity of the flow is slower in a region with a higher parameter κ^{-1}. If the velocity is slow in one part of the region, we refer this region as a slow region and the flow as a slow flow, similar to a faster region and a faster flow. When the value of the parameter κ^{-1} is very small (of order 1), then the flow in this region behaves as the Stokes flow, and we refer it as a free flow. Our first test is a faster Darcy flow going through the slower region; the second is a slower Darcy flow past a faster Darcy flow regions; the third is a free flow going across the Darcy flow region; and the last test is a Darcy flow passing the free flow region. All the numerical results indicate that the proposed GMsFEM is robust and accurate.

The rest of the paper is organized as follows. In Section 2, we present preliminaries on the Brinkman model and the GMsFEM. The construction of the coarse spaces for the GMsFEM is displayed in Section 3. In Section 4, numerical results for several representative examples are showed. The proofs of our main results, including stability and a priori error estimates, are exhibited in Section 5. Finally, we conclude our paper with some remarks in Section 6.

2. Preliminaries

In this section, we first present in detail the Brinkman problem we are dealing with, and the corresponding fine-scale discretization of this problem. Then we discuss briefly the multiscale strategy of solving this problem.

Now we describe the Brinkman model in a more detailed manner. Let Ω be a polygonal domain in $\mathbb{R}^d$ ($d = 2, 3$) with a boundary $\partial\Omega$. Then the Brinkman model reads: find $(u, p) \in H^1(\Omega)^d \times L_0^2(\Omega)$ such that

$$\nabla p - \mu\Delta u + \kappa^{-1}u = f \quad \text{in } \Omega, \tag{1a}$$
$$\operatorname{div} u = 0 \quad \text{in } \Omega, \tag{1b}$$
$$u = g \quad \text{on } \partial\Omega. \tag{1c}$$

Here the source term $f \in (L^2(\Omega))^d$, the boundary condition $g \in (H^{\frac{1}{2}}(\partial\Omega))^d$, and κ^{-1} is a positive definite heterogeneous tensor field with high-contrast. Without loss of generality, we assume the viscosity parameter $\mu = 1$ and $g = 0$ throughout.

To simplify the notation, we denote by $V(\Omega) = (H_0^1(\Omega))^d$ and $W(\Omega) = L_0^2(\Omega)$. The variational formulation of the problem is given by: find $u \in V(\Omega)$ and $p \in W(\Omega)$ such that

$$a(u, v) + b(v, p) = l_f(v) \quad \text{for all } v \in V(\Omega),$$
$$b(u, q) = 0 \quad \text{for all } q \in W(\Omega),$$

where the bilinear forms $a(\cdot, \cdot)$ and $b(\cdot, \cdot)$ are respectively defined by

$$a(u, v) = \langle \nabla u, \nabla v\rangle_\Omega + \left\langle \kappa^{-1}u, v\right\rangle_\Omega, \quad \text{for all } u, v \in V(\Omega),$$
$$b(u, p) = \langle \operatorname{div} u, p\rangle_\Omega, \quad \text{for all } u \in V(\Omega),\ p \in W(\Omega),$$

and the linear form l_f is given by

$$l_f(v) = \langle f, v\rangle_\Omega, \quad \text{for all } v \in V(\Omega),$$

where $\langle\cdot,\ \cdot\rangle_\Omega$ denotes the L^2 inner product over Ω.

We now turn our attention to a numerical approximation of the Brinkman problem (1). After writing the variational formulation we introduce a mixed finite element discretization for the approximation of velocities and pressures. Due to the nature of this multiscale problem we consider the framework of multiscale finite element method. the idea is computing upon the coarse grid for a coarse solution and then projecting this coarse scale solution to the fine grid. In the following, we introduce the necessary concepts and notations.

Let $\mathcal{T}_H$ be a coarse-grid partition of the domain Ω and $\mathcal{T}_h$ be a conforming fine triangulation of Ω. We assume that $\mathcal{T}_h$ is a refinement of $\mathcal{T}_H$, where h and H represent the mesh size of a fine and coarse cell respectively. Typically we assume that $0 < h \ll H < 1$, and that the triangulation $\mathcal{T}_h$ is fine enough to fully resolve the spatial variations of the coefficient κ while H is too coarse to accurately resolve this spatial variations inside a coarse element, and the coefficient κ may have large variations within the coarse block. On the triangulation $\mathcal{T}_h$, we introduce the following finite element spaces

$$V_h := \{v \in V(\Omega) | v|_K \in (P^2(K))^d \text{ for all } K \in \mathcal{T}_h\},$$
$$W_h := \{q \in W(\Omega) | w|_K \in P^0(K),\ \text{for all } K \in \mathcal{T}_h\}.$$

The standard mixed finite element method for problem (1) is to seek an approximation (u_h, p_h) in the finite element space $V_h \times W_h \subset V(\Omega) \times W(\Omega)$ such that

$$a(u_h, v) + b(v, p_h) = l_f(v) \quad \text{for all } v \in V_h,$$
$$b(q, u_h) = 0 \quad \text{for all } q \in W_h,$$

or which is equivalent to the solution of the following linear system

$$\begin{pmatrix} A & B \\ B^T & 0 \end{pmatrix} \begin{pmatrix} u \\ p \end{pmatrix} = \begin{pmatrix} F \\ 0 \end{pmatrix}.$$

Here the matrices denote

$$v^T A u = a(u, v), \quad \text{for all } u, v \in V_h, \tag{2}$$
$$q^T B u = b(u, q), \quad \text{for all } u \in V_h \text{ and } q \in W_h. \tag{3}$$

Note that here and below, in order to simplify notation, we are using the same notation for finite element functions and their corresponding vector representations.

It is well known the mixed finite element formulation described above is stable; see for instance [8]. In the case of high-contrast media, a very refined grid is needed in order to fully resolve small scale features, and thus it is prohibitively expensive to solve the resulting system. Meanwhile, if we naively apply P^2/P^0 finite element spaces over the coarse mesh $\mathcal{T}_H$, the resulting system is small but obviously the solution can only represent a poor approximation to the exact solution. To turn around the dilemma, we follow the GMsFEM framework proposed in [19].

In the GMsFEM methodology one divides the computations into offline and online computations. The offline computations are based upon a preliminary dimension reduction of the fine-grid finite element spaces (that may include dealing with additionally important physical parameters, uncertainties and nonlinearities), and then the online procedure (if needed) is applied to construct a reduced order model on the offline space. We start by constructing offline spaces.

We construct the coarse function space

$$V^{\text{off}} := \text{span}\{\phi_i\}_{i=1}^{N_c},$$

where N_c is the number of coarse basis functions. Each ϕ_i is supported in some coarse neighborhood w_l. For the pressure field p, we use the space of piecewise constant functions over the coarse triangulation $\mathcal{T}_H$, that is,

$$W^{\text{off}} := \{q \in L_0^2(\Omega) | q|_K \in P^0(K), \text{ for all } K \in \mathcal{T}_H\}. \tag{4}$$

We denote $N_H = \dim W^{\text{off}}$.

The idea is then to work on the reduced spaces $V^{\text{off}} \times W^{\text{off}}$ instead of the original spaces $V(\Omega) \times W(\Omega)$. In the general GMsFEM methodology, these offline spaces are used in the online computations where a further reduction may be performed; see [15,19] for details. The overall performance of the resulting GMsFEM depends on the approximation properties of the resulting offline and online coarse spaces. In this paper we focus on the construction of the offline spaces only. We mention that this is sufficient for the effective numerical upscaling of the Brinkman model proposed above where neither parameters or nonlinearities are considered. The more general case with additional parameters can also be studied using the proposed method, but it requires online dimension reduction [15,19,25] and thus defer to a future study.

The GMsFEM seeks an approximation $(u_0, p_0) \in V^{\text{off}} \times W^{\text{off}}$ which satisfies the coarse scale offline formulation,

$$a(u_0, v) + b^t(p_0, v) = l_f(v) \quad \text{for all } v \in V^{\text{off}}, \tag{5a}$$

$$b(u_0, q) = 0 \quad \text{for all } q \in W^{\text{off}}. \tag{5b}$$

We can interpret the method in the following way using matrix representations. Recall that both coarse basis functions $\{\phi_i\}_{i=1}^{N_c}$ and $\{q_i\}_{i=1}^{N_H}$ are defined on the fine grid, and can be represented by the fine grid basis functions. Specifically, we introduce the following matrices:

$$R_0^T = [\phi_1, \ldots, \phi_{N_c}], \qquad Q_0^T = [q_1, \ldots, q_{N_H}],$$

where we identify the basis ϕ_i and q_i with their coefficient vectors in the fine grid basis. Then the matrix analogue of the system (5) can be equivalently written as

$$\begin{pmatrix} R_0 A R_0^T & R_0 B Q_0^T \\ Q_0 B^T R_0^T & 0 \end{pmatrix} \begin{pmatrix} u_0 \\ p_0 \end{pmatrix} = \begin{pmatrix} R_0 F \\ 0 \end{pmatrix}. \tag{6}$$

Further, once we solve the coarse system (6), we can recover the fine scale solution by $R_0^T u_0$. In other words, R_0^T can be regarded as the transformation (also known as interpolation, extension, and downscaling) matrix from the space V^{off} to the space V^h.

The accuracy of the GMsFEM relies crucially on the coarse basis functions $\{\phi_i\}$. We shall present one novel construction of suitable basis functions for the Brinkman equation in Section 3.

3. The construction of the space V^{off}

In this section, we present the construction of the space V^{off} in detail. For the sake of simplicity, here we only consider the 2D case, the extension to 3D is natural but with more details involved. For the pressure field p, we simply use piecewise constant functions over the coarse grid as defined in (4). Therefore the focus below is on the construction of the offline velocity space V^{off}. To this end, we first introduce the concept of (harmonic) extension of boundary data in the Brinkman sense, which will play an important role in the construction. The precise definition is given below.

Definition 3.1 (*Brinkman Extension*)**.** For a domain $D \subset \mathbb{R}^d$, we define the Brinkman extension of any $v \in (H^{\frac{1}{2}}(\partial D))^d$, denoted by $\mathcal{H}(v) \in (H^1(D))^d$, to be the unique solution of the following homogeneous Brinkman equation (with $|D|$ being the measure of D)

$$\begin{aligned} &\nabla p - \mu \Delta \mathcal{H}(v) + \kappa^{-1} \mathcal{H}(v) = 0 \quad \text{in } D, \\ &\text{div } \mathcal{H}(v) = \frac{1}{|D|} \int_{\partial D} v \cdot n \quad \text{in } D, \\ &\mathcal{H}(v) = v \quad \text{on } \partial D. \end{aligned}$$

Remark 3.2. In practice, the extension $\mathcal{H}(v)$ is the numerical solution of the equation in the fine-scale finite element space $V_h(D) \times W_h(D)$, where D is a coarse block (see Fig. 1 for an illustration of coarse block and coarse neighborhood). This computation can be efficiently performed due to the moderated size of the coarse regions. Besides, the computations can be carried out in parallel, if the computations are required over all coarse regions.

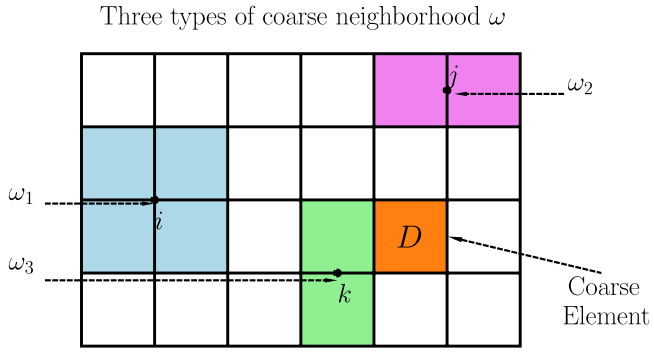

Fig. 1. Illustration of three types of coarse neighborhoods and coarse element: ω_i, $i = 1$, 2 and 3 corresponds to three types of partition of unity functions. The first type of partition of unity function has value 1 on i with support ω_1, similar to the second type and the third type of partition of unity functions.

Now we are ready to state the detailed construction of the offline velocity space V^{off}. Our construction consists of the following three steps. We defer the analysis of the resulting GMsFEM method to Section 5.

Step 1: Building multiscale partition of unity functions. First we introduce a set of generalized global partition of unity functions on the coarse grid. We denote the set of all coarse edges by $\mathcal{E}_H$, and consider the following finite element space:

$$M_H := \{v \in C^0(\mathcal{E}_H) : \ v|_F \in P^2(F), \ \text{for all } F \in \mathcal{E}_H\}.$$

Let $\mathcal{P}_H$ be the set of the shape functions of the space M_H. Then $\mathcal{P}_H$ also forms a partition of unity functions over the skeleton $\mathcal{E}_H$.

Next we introduce the set of multiscale partition of unity functions for a two-dimensional domain Ω. We remark that the construction for the three-dimensional case is similar. For any $\chi \in \mathcal{P}_H$, let ω denote the support of χ, and we call ω a coarse neighborhood associated with χ. In Fig. 1, we sketch all three possible types of the coarse neighborhood, ω_1, ω_2 and ω_3, respectively. ω_1 corresponds to partition of unity function χ having nodal value 1 at the coarse node i; ω_2 represents the support of χ valuing 1 at node j, and ω_3 stands for support of χ equaling to 1 at node k.

For each $\chi \in \mathcal{P}_H$, we have two Brinkman extensions of χ : $\mathcal{H}(\chi^x)$ and $\mathcal{H}(\chi^y)$. Here $\mathcal{H}(\chi^x)$ is the Brinkman extension of the Dirichlet data $\chi^x = (\chi, 0)$, and it is defined on each coarse block $D \subset \omega$. The extension $\mathcal{H}(\chi^y)$ is defined similarly, with $\chi^y = (0, \chi)$. We note that these vector functions can be extended by 0 to the entire domain Ω, since χ vanishes over $\partial\omega$. Finally, the generated partition of unity functions associated with χ is $\chi_x = \frac{1}{2}(\mathcal{H}(\chi^x))_x$, $\chi_y = \frac{1}{2}(\mathcal{H}(\chi^y))_y$, where $(\cdot)_x$ and $(\cdot)_y$ denote the first component and second component of a vector, respectively. Thus, for each $\chi \in \mathcal{P}_H$, we generate two partition of unity functions supported on ω. All these extensions together form a set of multiscale partition of unity functions, which are denoted by:

$$\mathcal{P}_{\text{ext}} = \{\chi_i\}_{i=1}^{N_p},$$

where N_p is the number of multiscale partition of unity functions. We note that the set $\mathcal{P}_{\text{ext}}$ does not have the default property of partition of unity over the domain Ω, but only over the skeleton $\mathcal{E}_H$, i.e.,

$$\sum_{i=1}^{N_p} \chi_i \equiv 1 \quad \text{on } \mathcal{E}_H. \tag{7}$$

Step 2: Constructing local snapshot space V^{ω}_{snap}. In this step, we construct the local snapshot spaces. Proceeding as before, for each $\chi \in \mathcal{P}_{ext}$, we let ω denote its support set, and call it the coarse neighborhood associated with χ, which consists of either two or four coarse blocks, cf. Fig. 1. The construction of the local snapshots is further divided into two substeps: generating the snapshot space over all coarse neighborhoods ω and then improving their linear independence.

Step 2.1. Computing snapshots: For each coarse neighborhood ω, let $J_h(\partial\omega)$ denote the set of fine nodes on $\partial\omega$. Let $\delta_k \in C^0(\partial\omega)$ denote the shape function associated with the node $x_k \in J_h(\partial\omega)$. i.e., $\delta_k \in C^0(\partial\omega)$ is the piecewise linear function that takes value 1 on the node x_k and vanishes on all other nodes. For each δ_k, it generates two Brinkman extensions:

$$\psi_{k,x} = \mathcal{H}((\delta_k, 0)) \quad \text{and} \quad \psi_{k,y} = \mathcal{H}((0, \delta_k)).$$

Now the raw snapshot space on ω is given by

$$\widetilde{V}^{\omega}_{\text{snap}} = \text{span}\{\psi_{i,x}, \psi_{i,y} : \ \text{for all } x_i \in J_h(\partial\omega)\} + \text{span}\{(1, 0), (0, 1)\}.$$

Here we artificially add two constant vectors in the basis; see Remark 3.3 below for the discussions.

Step 2.2: Improving linear independence of snapshots: After obtaining a family of local functions for each coarse neighborhood, we need to discard the possible linearly dependent local snapshots. To this end, we use a spectral problem based on the Euclidean inner product. Specifically, let U be a matrix with columns being the local snapshots vector representation.

We extract the important modes of U through the spectral decomposition of U^TU. In this manner, we keep the linearly independent snapshots for each coarse neighborhood ω and denote the resulting space by

$$V^{\omega}_{\text{snap}} = \text{span}\{\psi_l^{\omega,\text{snap}} : 1 \leq l \leq L^{\omega}\},$$

with L^{ω} being the number of local basis functions for the coarse neighborhood ω.

Step 3: Building the offline space V^{off}. In this final step, we build the global offline space V^{off} from the snapshot spaces V^{ω}_{snap}, and it involves two substeps: constructing local offline space and constructing global offline space.

Step 3.1: Local multiscale space $\widetilde{V}^{\omega}_{\text{off}}$. The idea at this step is to extract only important information from the computed local snapshots V^{ω}_{snap} corresponding to each coarse neighborhood ω. This can be achieved by performing a dimension reduction procedure in the space V^{ω}_{snap}. Namely, we consider the following spectral eigenvalue problem:

$$A\widehat{\Psi}_k^{\omega,\text{off}} = \lambda_k S\widehat{\Psi}_k^{\omega,\text{off}}, \tag{8}$$

where the matrices A and S are defined by

$$A = [a_{mn}] = \int_{\omega} \kappa(x)\nabla\psi_m^{\omega,\text{snap}} \cdot \nabla\psi_n^{\omega,\text{snap}}, \quad 1 \leq m, n \leq L^{\omega}$$
$$S = [s_{mn}] = \int_{\omega} \kappa(x)\psi_m^{\omega,\text{snap}}\psi_n^{\omega,\text{snap}}, \quad 1 \leq m, n \leq L^{\omega}.$$

Then we reorder the eigenvalues λ_k in an ascending order, and denote $\widehat{\Psi}_k^{\omega,\text{off}}$ as the corresponding eigenvectors.

To generate the offline space, we then choose the M_{off} smallest eigenvalues of (8) and the corresponding eigenvectors in the respective space of snapshots by setting $\widetilde{\Psi}_k^{\omega,\text{off}} = \sum_j \widehat{\Psi}_{kj}^{\text{off}}\psi_j^{\omega,\text{snap}}$, where $\widehat{\Psi}_{kj}^{\text{off}}$ are the coordinates of the vector $\widehat{\Psi}_k^{\omega,\text{off}}$. We then construct the offline space $\widetilde{V}^{\omega}_{\text{off}}$ corresponding to the coarse neighborhood ω as

$$\widetilde{V}^{\omega}_{\text{off}} = \text{span}\left(\widetilde{\Psi}_1^{\omega,\text{off}}, \ldots, \widetilde{\Psi}_{M_{\text{off}}}^{\omega,\text{off}}\right).$$

We note that this step is performed only on each coarse neighborhood ω. The dimensionality of the space $\widetilde{V}^{\omega}_{\text{off}}$ solely depends on the eigenvalue problem (8) within the neighborhood ω. It is known that this space is related to important features of the media (cf. [15]) such as high-conductivity channels and inclusions, and thus its dimensionality depends on the structure of the heterogeneities.

Remark 3.3. In the construction of the local snapshot space, we have added constant functions in addition to spectral basis functions. Hence, the constant function, which is the eigenvectors corresponding to the zero eigenvalue of (8), will always be in the offline space. By the construction of the offline space, each offline space contains the partition of unity functions, and the smallest offline space consists of those partition of unity functions only. This will be crucial in the stability analysis of the methods in Section 5.

Step 3.2: Construction of the global offline space V^{off} **by partition of unity.** The local multiscale spaces $\widetilde{V}^{\omega}_{\text{off}}$ are defined only on each neighborhood ω. However, it is not conforming if we simply extend the functions by 0 to the whole domain. We obtain a global conforming offline space V^{off} as follows.

First, we multiply each local offline space $\widetilde{V}^{\omega}_{\text{off}}$ by the corresponding partition of unity function χ:

$$\chi\widetilde{V}^{\omega}_{\text{off}} = \text{span}\left(\chi\widetilde{\Psi}_1^{\omega,\text{off}}, \ldots, \chi\widetilde{\Psi}_{M_{\text{off}}}^{\omega,\text{off}}\right).$$

Then the space $\chi\widetilde{V}^{\omega}_{\text{off}} \subset H_0^1(\omega)$, and we can extend the functions in $\chi\widetilde{V}^{\omega}_{\text{off}}$ to the whole domain Ω by zero, which is still denoted as $\chi\widetilde{V}^{\omega}_{\text{off}}$. Finally, we need to make a correction of the divergence of the resulting functions to satisfy the following condition:

$$\nabla \cdot V^{\text{off}} \subset W^{\text{off}}.$$

To this end, for each basis function $\chi\widetilde{\Psi}_i^{\omega,\text{off}}$, within each coarse block $D \subset \omega$, we keep its trace along ∂D and modify its interior values to be the Brinkman extension $\mathcal{H}(\chi\widetilde{\Psi}_i^{\omega,\text{off}}|_{\partial D})$. We denote this modified space by $\mathcal{H}(\chi\widetilde{V}^{\omega}_{\text{off}})$. The global offline space V^{off} results from assembling all these modified local spaces as:

$$V^{\text{off}} := \{v \in (H_0^1(\Omega))^d : v|_{\omega} \in \mathcal{H}(\chi\widetilde{V}^{\omega}_{\text{off}})\}.$$

This completes the construction of the offline space V^{off}. Finally, we refer to Section 2 for the coupling of the offline basis functions.

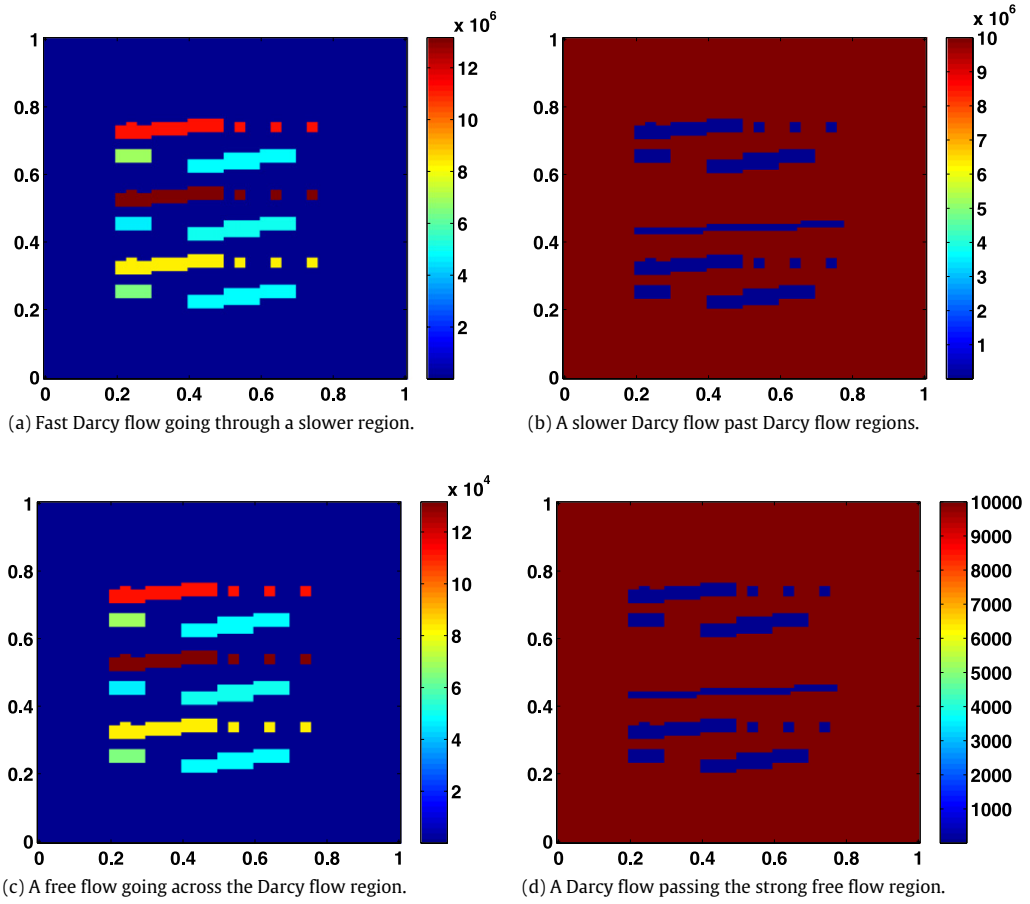

(a) Fast Darcy flow going through a slower region.

(b) A slower Darcy flow past Darcy flow regions.

(c) A free flow going across the Darcy flow region.

(d) A Darcy flow passing the strong free flow region.

Fig. 2. Four representative inverse permeability fields κ^{-1}.

4. Numerical results

Now we test our framework with several examples. In our experiments, we take the domain $\Omega = [0, 1] \times [0, 1]$, the source term $f = 0$, $\mu = 1$, and the boundary condition is the constant horizontal velocity:

$$g = (1, 0) \quad \text{on } \partial\Omega.$$

We study the model with different high-contrast parameter κ^{-1} depicted in Fig. 2. Recall that the velocity of the flow is slower in a region with a higher parameter κ^{-1}. If the velocity is slow in one part of the region, we refer this region as a slow region and the flow as a slow flow, similar to a faster region and a faster flow. When the value of the parameter κ^{-1} is very small (of order 1), then the flow in this region behaves as the Stokes flow, and we refer it as a free flow. Fig. 2(a) shows a faster Darcy flow going through the slower region; in Fig. 2(b), we exposit a slower Darcy flow past a faster Darcy flow regions; in Fig. 2(c), a free flow going across the Darcy flow region is represented; and in Fig. 2(d), a Darcy flow passing the free flow region is shown.

We divide the computational domain $\Omega = [0\ 1] \times [0\ 1]$ into $N_f = 1/h^2$ equal squares (where each square is further divided into two triangles), and use P_2/P_0 elements on the fine mesh with $h = 1/100$. We use a coarse-mesh size $H = 1/10$ where we divide the domain $\Omega = [0, 1] \times [0, 1]$ into $1/H^2$ squares.

We depict the fine-scale solution, and three coarse-scale solutions with coarse spaces of dimensions 798, 1110 and 2726 in Fig. 3. The dimension of the fine scale velocity space V_h is 80 802. In these numerical tests, we use the value of the permeability field κ^{-1} from Fig. 2(a). We observe that a larger coarse space yields a better approximation of the fine-scale solution. Further, we have the following observations.

(a) The use of one single basis function for each node gives large errors and thus it is necessary to add spectral basis functions.
(b) The error decreases as more spectral basis functions are added in each coarse-grid block.
(c) The error decreases if the solution displays fast flow in some regions instead of Darcy flow over the whole region under the same contrast.

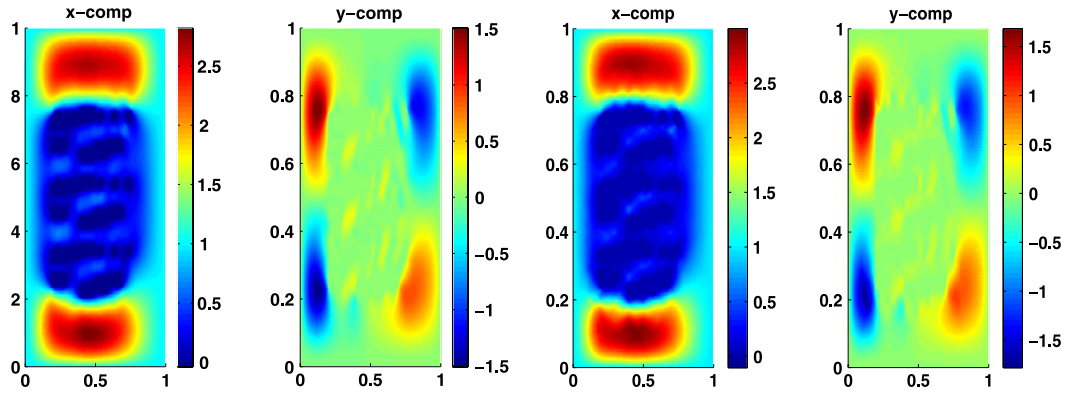

(a) Fine-scale solution. (b) Coarse solution with solution space of 798.

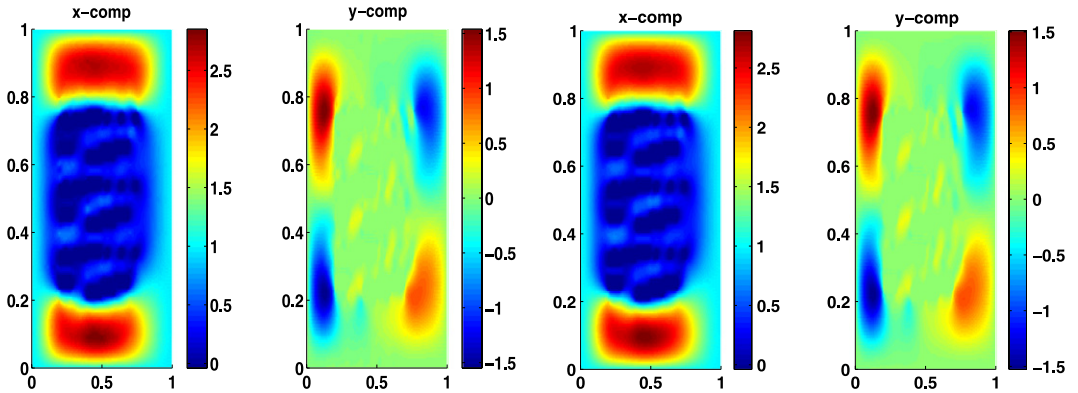

(c) Coarse solution with solution space of 1110. (d) Coarse solution with solution space of 2726.

Fig. 3. The fine-scale solution and three coarse-scale solutions with different dimensions of coarse spaces using the permeability field κ^{-1} in Fig. 2(a).

Table 1
Numerical results for problem (1) with κ^{-1} in Fig. 2(a). The L^2-weighted error and energy error are 66.34% and 99.73% for the MsFEM solution. In the simulation, the dimension of the snapshot space is fixed at 4498 with a weighted L^2 and energy relative error 1.26% and 2.13%.

$\dim(V_{\text{off}})$	$\|u - u^{\text{off}}\|$ (%)	
	$L^2_\kappa(D)$	$H^1_\kappa(D)$
888	35.46	74.91
1372	26.62	58.25
2028	11.79	26.05
2204	8.61	19.47

In Tables 1–4, we present the results with the multiscale partition of unity functions as required by the conforming Galerkin formulation corresponding to permeability fields in Fig. 2. In the tables, the first column shows the dimension of the offline space V^{off}, and the L^2-weighted error between the offline solution u^{off} and the fine-scale solution u and the H^1-weighted energy error are calculated respectively by

$$\|u - u^{\text{off}}\|_{L^2_\kappa(D)} = \frac{\left\|\kappa^{-1/2}(u - u^{\text{off}})\right\|_{L^2(\Omega)}}{\left\|\kappa^{-1/2}u\right\|_{L^2(\Omega)}} \quad \text{and} \quad \|u - u^{\text{off}}\|_{H^1_\kappa(D)} = \frac{\left\|\kappa^{-1/2}\nabla(u - u^{\text{off}})\right\|_{L^2(\Omega)}}{\left\|\kappa^{-1/2}\nabla u\right\|_{L^2(\Omega)}}.$$

In Table 1, we display the velocity error results using a permeability field with values of κ^{-1} large in the background, with small inclusions values, cf. Fig. 2(a). For simplicity, we set a threshold value λ^{off} for selecting eigenvectors in the construction of the offline space. Specifically, for each coarse neighborhood ω, the offline space consists of those eigenvectors in Eq. (8) with eigenvalues $\lambda_k \geq \lambda^{\text{off}}$. Notice that the smaller is λ^{off}, the larger is the velocity offline space. In the simulation, the choices $\lambda^{\text{off}} = 1/3, 1/4, 1/7$, and $1/10$ give the offline spaces of dimension 888, 1372, 2028 and 2204, respectively. It is observed from Table 1 that the error decreases from 74.91% to 19.47%.

Table 2
Numerical results for problem (1) with κ^{-1} in Fig. 2(b). The L^2-weighted error and energy error are 74.68% and 130.42% for the MsFEM solution. In the simulation, the dimension of the snapshot space is fixed at 4498 with a weighted L^2 and energy relative error 1.33% and 13.03%.

$\dim(V_{\text{off}})$	$\|u - u^{\text{off}}\|$ (%)	
	$L^2_\kappa(D)$	$H^1_\kappa(D)$
682	7.86	36.90
1512	1.85	18.37
2230	1.51	15.27
2744	1.38	13.84

Table 3
Numerical results for problem (1) with κ^{-1} in Fig. 2(c). The L^2-weighted error and energy error are 85.25% and 73.85% for the MsFEM solution. In the simulation, the dimension of the snapshot space is fixed at 4498 with a weighted L^2 and energy relative error 1.94% and 3.54%.

$\dim(V_{\text{off}})$	$\|u - u^{\text{off}}\|$ (%)	
	$L^2_\kappa(D)$	$H^1_\kappa(D)$
834	35.58	38.10
1512	14.34	19.41
2084	6.81	9.90
2306	4.54	7.65

Table 4
Numerical results for problem (1) with κ^{-1} in Fig. 2(d). The L^2-weighted error and energy error are 74.68% and 130.42% for the MsFEM solution. In the simulation, the dimension of the snapshot space is fixed at 4498 with a weighted L^2 and energy relative error 1.47% and 3.75%.

$\dim(V_{\text{off}})$	$\|u - u^{\text{off}}\|$ (%)	
	$L^2_\kappa(D)$	$H^1_\kappa(D)$
682	46.80	43.26
1090	30.92	30.30
1992	13.49	13.15
3344	6.36	5.38

The results in Table 2 are calculated with values of κ^{-1} that are large in inclusions, and small in the background, cf. Fig. 2(b). Compared with results in Table 1, the errors in Table 2 are slightly better in the sense that the relative energy errors are smaller when using the same dimensional offline space. In this numerical test, we take $\lambda^{\text{off}} = 1/3$, $1/4$, $1/7$, and $1/10$ with the offline space of dimension 682, 1512, 2230 and 2744 respectively. From Table 2, the energy errors decrease from 36.90% to 13.84%.

In Tables 3 and 4, we employ certain permeability fields κ^{-1} to get fast flow and Darcy flow simultaneously. In Table 3, we use a permeability field κ^{-1} small in inclusions, and large in the background, cf. Fig. 2(c). In this numerical test, we take $\lambda^{\text{off}} = 3$, 4, 7, and 10 with the offline space of dimension 834, 1512, 2084 and 2316 respectively. From Table 2, the energy errors decrease from 38.10% to 7.65%. In Table 4, we experimented with values of κ^{-1} large in inclusions, and small in the background as shown in Fig. 2(d). In this numerical test, we take $\lambda^{\text{off}} = 3$, 4, 7, and 10 with the offline space of dimension 682, 1090, 1992 and 3344 respectively. From Table 2, the energy errors decrease from 43.26% to 5.38%.

In Table 3, the solution represents fast flow in the inclusions (with high permeability value) and Darcy flow in the background, whereas in Table 4, the solution is a fast flow in the background (with high permeability value) and Darcy flow in the inclusions. The results in these four tables indicate that the errors are smaller when fast flow exists.

5. Convergence analysis

This section is dedicated to the stability and convergence analysis of our method. In particular, we present a priori error estimates for the method.

We first derive the stability arguments in the form of inf–sup conditions, and consequently show the approximation property of the method. We admit that the analysis of mixed finite elements for Brinkman (Stokes and Darcy) equations as well as similar models is now standard and the classical finite element method for Darcy equation have been analyzed in the literature [16]. Nevertheless, as mentioned in the introduction, upscaling methods for Brinkman model are difficult to design and analyze. In this section we combine numerical analysis of mixed finite elements methods (for the Brinkman equation) with the analysis of GMsFEM procedures to obtain approximation results of our methods.

For the sake of simplicity, we assume a homogeneous boundary condition $g = 0$ in the Brinkman equation (1).

5.1. Stability argument

To prove the stability of the method, we apply the well known *inf–sup* argument. First, we define a norm on $V(\Omega)$ by

$$|||u|||^2_{\mathrm{V},\Omega} = a(u,u) + M\,\langle \mathrm{div}\, u, \mathrm{div}\, u\rangle_\Omega\,, \tag{9}$$

and the norm on $W(\Omega)$ is defined by

$$|||p|||_{\mathrm{P},\Omega} = M^{-\frac{1}{2}}\,\|p\|_{L^2(\Omega)}\,, \tag{10}$$

where $M = \max\left(\left\|\kappa^{-1}\right\|_{L^\infty(\Omega)},\ 1\right)$. We also define the following two null spaces:

$$Z := \{v \in V(\Omega):\ b(v,p) = 0,\ \text{for all}\ \ p \in W(\Omega)\},$$
$$Z^{\mathrm{off}} := \{v \in V^{\mathrm{off}}:\ b(v,p) = 0,\ \text{for all}\ \ p \in W^{\mathrm{off}}\}.$$

Under these definitions and the construction of V^{off} and W^{off}, it holds:

$$Z^{\mathrm{off}} \subset Z, \qquad a(v,v) \succeq |||v|||_{\mathrm{V},\Omega} \quad \text{for all } v \in Z. \tag{11}$$

Here, and in what follows, we use the notation $A \succeq B$ to represent $A \geq \mathcal{C}B$ with a constant $\mathcal{C}$ independent of the contrast and the functions involve, and a similar interpretation applies to the notation $\preceq$. The above two results imply that the bilinear form $a(\cdot,\cdot)$ is also coercive on Z^{off}.

We first verify that the continuous problem (1) satisfies the *inf–sup* condition.

Lemma 5.1. *Let $|||\cdot|||_{\mathrm{V},\Omega}$ and $|||\cdot|||_{\mathrm{P},\Omega}$ be defined in (9) and (10). Then the following inf–sup condition holds independent of the contrast*

$$\sup_{v\in V(\Omega)\setminus\{0\}} \frac{\langle \mathrm{div}\, v, q\rangle_\Omega}{|||v|||_{\mathrm{V},\Omega}} \succeq |||q|||_{\mathrm{P},\Omega}, \quad \textit{for all } q \in W(\Omega). \tag{12}$$

Proof. It is well known [26] that the operator $b(\cdot,\cdot)$ satisfies the *inf–sup* condition under the standard norms, i.e.,

$$\sup_{v\in V(\Omega)\setminus\{0\}} \frac{\langle \mathrm{div}\, v, q\rangle_\Omega}{\|v\|_{H^1(\Omega)}} \succeq \|q\|_{L^2(\Omega)}\,, \quad \text{for all } q \in W(\Omega). \tag{13}$$

By the definition of $|||\cdot|||_{\mathrm{V},\Omega}$ and $|||\cdot|||_{\mathrm{P},\Omega}$, we have $|||v|||_{\mathrm{V},\Omega} \preceq M^{\frac{1}{2}}\,\|v\|_{H^1(\Omega)}$, and $\|q\|_{L^2(\Omega)} = M^{\frac{1}{2}}|||q|||_{\mathrm{P},\Omega}$ for all $(v,q) \in V(\Omega)\times W(\Omega)$. Combining these facts with (13) completes the proof. □

Next, we show that the discrete problem (5) also satisfies this type of inf–sup condition with a constant independent of the contrast for every offline space $V^{\mathrm{off}} \times W^{\mathrm{off}}$. First, we consider the following auxiliary space:

$$V_H(\Omega) := \{v \in H^1(\Omega) | v|_K \in Q^2(K),\ \forall K \in \mathcal{T}_H\},$$
$$W_H(\Omega) := \{q \in L^2_0(\Omega) | q|_K \in Q^0(K),\ \forall K \in \mathcal{T}_H\}.$$

For the Brinkman equation, we have the following inf–sup condition in $V_H(\Omega)\times W_H(\Omega)$ (see [27]),

$$\sup_{v\in V_H(\Omega)\setminus\{0\}} \frac{\langle \mathrm{div}\, v, q\rangle_\Omega}{\|v\|_{H^1(\Omega)}} \succeq \|q\|_{L^2(\Omega)}\,, \quad \text{for all } q \in W_H(\Omega). \tag{14}$$

Following the proof of Lemma 5.1, we can obtain the discrete inf–sup condition in $V_H(\Omega)\times W_H(\Omega)$ with $|||\cdot|||_{\mathrm{V},\Omega}$ and $|||\cdot|||_{\mathrm{P},\Omega}$, i.e.,

$$\sup_{v\in V_H(\Omega)\setminus\{0\}} \frac{\langle \mathrm{div}\, v, q\rangle_\Omega}{|||v|||_{\mathrm{V},\Omega}} \succeq |||q|||_{\mathrm{P},\Omega}, \quad \text{for all } q \in W_H(\Omega). \tag{15}$$

To prove the *inf–sup* condition for the space $V^{\mathrm{off}} \times W^{\mathrm{off}}$, we need the following result, which states the stability of the Brinkman extension with respect to the weighted norm defined in (9).

Lemma 5.2. *For any $w \in (H^1(D))^d$, the Brinkman extension $\mathcal{H}(w)$ of w on D satisfies*

$$|||\mathcal{H}(w)|||_{\mathrm{V},D} \preceq |||w|||_{\mathrm{V},D}. \tag{16}$$

Proof. By the definition of the Brinkman extension, $(\mathcal{H}(w), p) \in (H(D))^d \times L^2_0(D)$ satisfies

$$\nabla p - \Delta\mathcal{H}(w) + \kappa^{-1}\mathcal{H}(w) = 0, \quad \text{in } D,$$
$$\mathrm{div}\ \mathcal{H}(w) = \frac{\int_{\partial D} w\cdot n}{|D|} \quad \text{in } D,$$
$$\mathcal{H}(w) = w, \quad \text{on } \partial D.$$

Denote $v = \mathcal{H}(w) - w$, then v satisfies

$$\begin{aligned} &\nabla p - \Delta v + \kappa^{-1} v = \Delta w - \kappa^{-1} w, \quad \text{in } D, \\ &\operatorname{div} v = \frac{\int_{\partial D} w \cdot n}{|D|} - \operatorname{div} w \quad \text{in } D, \\ &v = 0, \quad \text{on } \partial D. \end{aligned} \tag{17}$$

Since $p \in L^2_0(D)$, by Lemma 11.2.3 in [27], there exists $\phi \in (H^1_0(D))^d$ such that

$$p = -\operatorname{div} \phi \quad \text{and} \quad \|\phi\|_{H^1(D)} \preceq \|p\|_{L^2(D)}. \tag{18}$$

Multiplying Eq. (17) by ϕ and integrating by parts, we obtain,

$$\langle p,\ p\rangle_D + \langle \nabla v,\ \nabla \phi\rangle_D + \left\langle \kappa^{-1} v,\ \phi\right\rangle_D = -\langle \nabla w,\ \nabla \phi\rangle_D - \left\langle \kappa^{-1} w,\ \phi\right\rangle_D.$$

Thus

$$\langle p,\ p\rangle_D = -\langle \nabla v,\ \nabla \phi\rangle_D - \left\langle \kappa^{-1} v,\ \phi\right\rangle_D - \langle \nabla w,\ \nabla \phi\rangle_D - \left\langle \kappa^{-1} w,\ \phi\right\rangle_D.$$

Using the Cauchy–Schwarz inequality and (18), we arrive at,

$$\begin{aligned} \|p\|^2_{L^2(D)} &\preceq \left(\|\nabla v\|_{L^2(D)} + \left\|\kappa^{-1} v\right\|_{H^{-1}(D)} + \|\nabla w\|_{L^2(D)} + \left\|\kappa^{-1} w\right\|_{H^{-1}(D)} \right) \|p\|_{L^2(D)} \\ &\preceq \left(\|\nabla v\|_{L^2(D)} + M \left\|\kappa^{-\frac{1}{2}} v\right\|_{L^2(D)} + \|\nabla w\|_{L^2(D)} + M \left\|\kappa^{-\frac{1}{2}} w\right\|_{L^2(D)} \right) \|p\|_{L^2(D)}. \end{aligned}$$

Then it yields the pressure estimate

$$\|p\|_{L^2(D)} \preceq \|\nabla v\|_{L^2(D)} + M \left\|\kappa^{-\frac{1}{2}} v\right\|_{L^2(D)} + \|\nabla w\|_{L^2(D)} + M \left\|\kappa^{-\frac{1}{2}} w\right\|_{L^2(D)}. \tag{19}$$

Multiplying Eq. (17) by v and integrating by parts, yields,

$$-\langle p, \operatorname{div} v\rangle_D + \langle \nabla v, \nabla v\rangle_D + \left\langle \kappa^{-1} v, v\right\rangle_D = \left\langle \Delta w - \kappa^{-1} w, v\right\rangle_D.$$

Using Cauchy–Schwarz inequality and the fact that p has zero mean on D, it follows that,

$$\begin{aligned} \langle \nabla v, \nabla v\rangle_D + \left\langle \kappa^{-1} v, v\right\rangle_D &= \left\langle \Delta w - \kappa^{-1} w, v\right\rangle_D + \langle p, \operatorname{div}\ v\rangle_D \\ &= \left\langle \Delta w - \kappa^{-1} w, v\right\rangle_D + \langle p, \operatorname{div}\ (\mathcal{H}(w) - w)\rangle_D \\ &= \left\langle \Delta w - \kappa^{-1} w, v\right\rangle_D - \langle p, \operatorname{div}\ w\rangle_D \\ &\le \|\nabla w\|_{L^2(D)} \|\nabla v\|_{L^2(D)} + \left\|\kappa^{-\frac{1}{2}} w\right\|_{L^2(D)} \left\|\kappa^{-\frac{1}{2}} v\right\|_{L^2(D)} + \|p\|_{L^2(D)} \|\operatorname{div} w\|_{L^2(D)}. \end{aligned}$$

Inserting the pressure estimate (19) and Young's inequality, we deduce

$$\begin{aligned} \langle \nabla v, \nabla v\rangle_D + \left\langle \kappa^{-1} v, v\right\rangle_D \preceq\ & \frac{1}{2\delta} \left(\|\nabla w\|^2_{L^2(D)} + \left\|\kappa^{-\frac{1}{2}} w\right\|^2_{L^2(D)} \right) + \frac{\delta}{2} \left(\|\nabla v\|^2_{L^2(D)} + \left\|\kappa^{-\frac{1}{2}} v\right\|^2_{L^2(D)} \right) \\ &+ \frac{\delta}{2M} \left(\|\nabla v\|^2_{L^2(D)} + M \left\|\kappa^{-\frac{1}{2}} v\right\|^2_{L^2(D)} + \|\nabla w\|^2_{L^2(D)} + M \left\|\kappa^{-\frac{1}{2}} w\right\|^2_{L^2(D)} \right) \\ &+ \frac{M}{2\delta} \|\operatorname{div} w\|^2_{L^2(D)}. \end{aligned}$$

Now the choice $\delta = \frac{1}{4}$ yields

$$\langle \nabla v, \nabla v\rangle_D + \left\langle \kappa^{-1} v, v\right\rangle_D \preceq \|\nabla w\|^2_{L^2(D)} + \left\|\kappa^{-\frac{1}{2}} w\right\|^2_{L^2(D)} + M \|\operatorname{div} w\|^2_{L^2(D)} = |\!|\!| w |\!|\!|^2_{\mathrm{V},D}.$$

Recall that $\mathcal{H}(w) = v + w$. By triangle inequality, we have

$$\langle \nabla \mathcal{H}(w), \nabla \mathcal{H}(w)\rangle_D + \left\langle \kappa^{-1} \mathcal{H}(w), \mathcal{H}(w)\right\rangle_D \preceq |\!|\!| w |\!|\!|^2_{\mathrm{V},D}.$$

It suffices to show

$$M^{\frac{1}{2}} \|\operatorname{div} \mathcal{H}(w)\|_{L^2(D)} \preceq |\!|\!| w |\!|\!|_{\mathrm{V},D}. \tag{20}$$

Indeed from the compatibility condition, we obtain: $\operatorname{div}\mathcal{H}(w) = \frac{1}{|D|}\int_D \operatorname{div} w$. Hence,

$$|\operatorname{div}\mathcal{H}(w)| = \left|\frac{1}{|D|}\int_D \operatorname{div} w\right| \leq \frac{1}{|D|}\int_D |\operatorname{div} w| \leq \|\operatorname{div} w\|_{L^2(D)}\,|D|^{-\frac{1}{2}},$$

where in the last step we used Cauchy–Schwarz inequality. Consequently

$$\|\operatorname{div}\mathcal{H}(w)\|^2_{L^2(D)} \preceq \|\operatorname{div} w\|^2_{L^2(D)}\,|D|^{-1}|D| = \|\operatorname{div} w\|^2_{L^2(D)}.$$

This completes the proof. □

We are now ready to show the *inf–sup* condition in the space $V^{\text{off}} \times W^{\text{off}}$.

Lemma 5.3. *For $|||\cdot|||_{\mathrm{V},\Omega}$ and $|||\cdot|||_{\mathrm{P},\Omega}$ defined in (9) and (10), we have the following inf–sup condition with inf–sup constant independent of the contrast*

$$\sup_{v\in V^{\text{off}}(\Omega)\setminus\{0\}} \frac{\langle \operatorname{div} v, q\rangle_\Omega}{|||v|||_{\mathrm{V},\Omega}} \succeq |||q|||_{\mathrm{P},\Omega}, \quad \textit{for all } q \in W^{\text{off}}(\Omega). \tag{21}$$

Proof. First note $W^{\text{off}} = W_H(\Omega)$. By (15), we have

$$\sup_{v\in V_H(\Omega)\setminus\{0\}} \frac{\langle \operatorname{div} v, q\rangle_\Omega}{|||v|||_{\mathrm{V},\Omega}} \succeq |||q|||_{\mathrm{P},\Omega}, \quad \text{for all } q \in W^{\text{off}}.$$

For any $v \in V_H(\Omega)$, let $\mathcal{H}(v)$ be the Brinkman extension of $v|_{\mathcal{E}_H}$, i.e., $\mathcal{H}(v)$ takes the value of v on the skeleton $\mathcal{E}_H$ and is extend to the interior by Brinkman extension within each coarse block. Then $v|_F \in [P^2(F)]^2$, $\forall F \in \mathcal{E}_H$. According to the construction of the offline space V^{off} in Section 3, we have

$$\mathcal{H}(v) \in V^{\text{off}}.$$

Moreover, for any $q \in W^{\text{off}}$, q is piecewise constant on each coarse block. By combining this fact and the definition of Brinkman extension, we have

$$\langle \operatorname{div} v, q\rangle_D = \langle \operatorname{div}\mathcal{H}(v), q\rangle_D,$$

for every coarse block D. Finally, we complete the proof by using Lemma 5.2:

$$\begin{aligned} |||q|||_{\mathrm{P},\Omega} &\preceq \sup_{v\in V_H(\Omega)\setminus\{0\}} \frac{\langle \operatorname{div} v, q\rangle_\Omega}{|||v|||_{\mathrm{V},\Omega}} = \sup_{v\in V_H(\Omega)\setminus\{0\}} \frac{\langle \operatorname{div}\mathcal{H}(v), q\rangle_\Omega}{|||v|||_{\mathrm{V},\Omega}} \\ &\preceq \sup_{v\in V_H(\Omega)\setminus\{0\}} \frac{\langle \operatorname{div}\mathcal{H}(v), q\rangle_\Omega}{|||\mathcal{H}(v)|||_{\mathrm{V},\Omega}} \preceq \sup_{v\in V^{\text{off}}(\Omega)\setminus\{0\}} \frac{\langle \operatorname{div} v, q\rangle_\Omega}{|||v|||_{\mathrm{V},\Omega}}. \quad \square \end{aligned}$$

Now by combining Lemma 5.1, Lemma 5.3 and (11), we obtain the following stability result, by repeating the proof of Theorem 3.2 in [8].

Theorem 5.4. *Let $(u,p) \in V(\Omega)\times W(\Omega)$ and $(u_0,p_0) \in V^{\text{off}}(\Omega)\times W^{\text{off}}(\Omega)$ be the Galerkin solutions of problem (1) and problem (5) respectively. We have*

$$|||u-u_0|||_{\mathrm{V},\Omega} \preceq \inf_{w\in V^{\text{off}}(\Omega)} |||u-w|||_{\mathrm{V},\Omega}. \tag{22}$$

5.2. Convergence results

Now we derive an error estimate for our method. To this end, we first give several basic estimates on the Brinkman extension.

Lemma 5.5. *For each partition of unity function χ_i with support ω_i, let $(u_c,p_c) \in (H^1(\omega_i))^d \times L^2_0(\omega_i)$ solve*

$$\begin{aligned} &\nabla p_c - \Delta u_c + \kappa^{-1}u_c = 0 \quad \textit{in } \omega_i, \\ &\operatorname{div} u_c = \frac{\int_{\partial\omega_i} g\cdot n}{|\omega_i|} \quad \textit{in } \omega_i, \\ &u_c = g \quad \textit{on } \partial\omega_i. \end{aligned}$$

Then the following a priori estimate holds

$$\int_{\omega_i} \chi_i^2 |\nabla u_c|^2 + \int_{\omega_i} \kappa^{-1} \chi_i^2 |u_c|^2 \preceq \int_{\omega_i} |\nabla \chi_i|^2 |u_c|^2 + \int_{\omega_i} \kappa^{-2} |u_c|^2 + \int_{\omega_i} |\operatorname{div} u_c|^2 + \|p_c\|^2_{L^2(\omega_i)} . \tag{23}$$

Proof. Multiplying the equation by $\chi_i^2 u_c$ yields

$$-\left\langle p_c, \operatorname{div}(\chi_i^2 u_c)\right\rangle_{\omega_i} + \left\langle \nabla u_c, \nabla(\chi_i^2 u_c)\right\rangle_{\omega_i} + \left\langle \kappa^{-1} u_c, \chi_i^2 u_c\right\rangle_{\omega_i} = 0.$$

Some simple algebraic manipulations give

$$\begin{aligned}
\int_{\omega_i} \chi_i^2 |\nabla u_c|^2 + \int_{\omega_i} \kappa^{-1} \chi_i^2 u_c^2 &= \langle p_c, 2\chi_i \nabla \chi_i \cdot u_c\rangle_{\omega_i} + \left\langle p_c, \chi_i^2 \operatorname{div} u_c\right\rangle_{\omega_i} - \langle \nabla u_c, 2\chi_i \nabla \chi_i \cdot u_c\rangle_{\omega_i} , \\
&\preceq \|p_c\|_{L^2(\omega_i)} \left(\|\nabla \chi_i \cdot u_c\|_{L^2(\omega_i)} + \|\operatorname{div} u_c\|_{L^2(\omega_i)}\right) \\
&\quad + \|\chi_i \nabla u_c\|_{L^2(\omega_i)} \|\nabla \chi_i \cdot u_c\|_{L^2(\omega_i)} , \\
&\preceq \frac{\delta}{2}\left(\|p_c\|^2_{L^2(\omega_i)} + \|\chi_i \nabla u_c\|^2_{L^2(\omega_i)}\right) + \frac{1}{2\delta}\left(\|\nabla \chi_i \cdot u_c\|^2_{L^2(\omega_i)} + \|\operatorname{div} u_c\|^2_{L^2(\omega_i)}\right).
\end{aligned}$$

Taking $\delta = \frac{1}{4}$, we obtain the desired inequality. □

Lemma 5.6. *Let $\omega_i \subset \mathcal{T}_H$ be an arbitrary coarse neighborhood. Let $(u_N, p_N) \in (H_0^1(\omega_i))^d \times L_0^2(\omega_i)$ solve*

$$\begin{aligned}
&\nabla p_N - \Delta u_N + \kappa^{-1} u_N = f \quad \text{in } \omega_i, \\
&\operatorname{div} u_N = 0 \quad \text{in } \omega_i, \\
&u_N = 0 \quad \text{on } \partial\omega_i.
\end{aligned}$$

Then there holds

$$|||u_N|||_{\mathrm{V},\omega_i} \preceq H \|f\|_{L^2(\omega_i)} . \tag{24}$$

Proof. By multiplying the first equation by u_N, integrating by parts and the divergence free property of u_N, we obtain

$$\|\nabla u_N\|^2_{L^2(\omega_i)} + \left\|\kappa^{-\frac{1}{2}} u_N\right\|^2_{L^2(\omega_i)} = \langle f, u_N\rangle_{\omega_i} .$$

In view of the boundary condition, we can apply Poincaré's inequality,

$$\|u_N\|_{L^2(\omega_i)} \preceq H \|\nabla u_N\|_{L^2(\omega_i)} .$$

Thus

$$\|\nabla u_N\|^2_{L^2(\omega_i)} + \left\|\kappa^{-\frac{1}{2}} u_N\right\|^2_{L^2(\omega_i)} = \langle f, u_N\rangle_{\omega_i} \preceq H \|\nabla u_N\|_{L^2(\omega_i)} \|f\|_{L^2(\omega_i)} .$$

Finally, we complete the proof by the Young's inequality. □

Now we are ready to state our main error estimate.

Theorem 5.7. *Let $\Lambda_* = \min_{\omega_i} \lambda^{\omega_i}_{L_i+1}$. Then*

$$|||u - u_0|||^2_{\mathrm{V},\Omega} \preceq \frac{1}{\Lambda_*} \|\nabla u\|^2_{L^2(\Omega)} + H^2 \|f(x)\|^2_{L^2(\Omega)} + \|p_c\|^2_{L^2(\Omega)}$$

where p_c is defined by (25) below.

Proof. In view of the linearity of the Eq. (1), on each coarse neighborhood $\omega_i \subset \mathcal{T}_H$, u can be decomposed into $u = \mathcal{H}(u) + u_N$, where $\mathcal{H}(u)$ is the Brinkman extension of u and u_N is the residual in Lemma 5.6. For each χ_i, let $I^0 u$ be the local interpolant of u in the local offline space $\tilde{V}^{\omega_i}_{\mathrm{off}}$. Then there exists $p_c \in L^2(\omega_i)$, s.t.

$$\begin{aligned}
&\nabla p_c - \Delta(u - I^0 u) + \kappa^{-1}(u - I^0 u) = 0 \quad \text{in } \omega_i, \\
&\operatorname{div}(u - I^0 u) = \frac{\int_{\partial\omega_i} h_i \cdot n}{|\omega_i|} \quad \text{in } \omega_i, \\
&(u - I^0 u) = h_i \quad \text{on } \partial\omega_i,
\end{aligned} \tag{25}$$

since $I^0 u$ equals 0 over $\partial\omega_i$ (the support of χ_i is ω_i) and each basis in $\tilde{V}^{\omega_i}_{\mathrm{off}}$ has the properties of divergence constant. Here, h_i denotes the boundary value of $u - I^0 u$ over $\partial\omega_i$.

By the construction of the offline space V^{off}, $\mathcal{H}(\chi_i I^0 u) \in V^{\text{off}}$. By Theorem 5.4, we have

$$\begin{aligned}
|||u-u_0|||^2_{\mathrm{V},\Omega} &\preceq \inf_{v\in V^{\text{off}}} |||u-v|||^2_{\mathrm{V},\Omega} \\
&\preceq \left|\left|\left| u-\sum_{i=1}^{N_C}\mathcal{H}(\chi_i I^0 u)\right|\right|\right|^2_{\mathrm{V},\Omega} \preceq \left|\left|\left| \mathcal{H}(u)-\sum_{i=1}^{N_c}\mathcal{H}(\chi_i I^0 u)\right|\right|\right|^2_{\mathrm{V},\Omega} + |||u_N|||^2_{\mathrm{V},\Omega}, \\
&\preceq \left|\left|\left| \mathcal{H}\left(\sum_{i=1}^{N_c}\chi_i u\right)-\sum_{i=1}^{N_c}\mathcal{H}(\chi_i I^0 u)\right|\right|\right|^2_{\mathrm{V},\Omega} + H^2\,\|f(x)\|^2_{L^2(\omega_i)}.
\end{aligned}$$

Here the last step follows from the estimate in Lemma 5.6. For the first term, we have

$$\begin{aligned}
\left|\left|\left| \mathcal{H}\left(\sum_{i=1}^{N_c}\chi_i u\right)-\sum_{i=1}^{N_c}\mathcal{H}(\chi_i I^0 u)\right|\right|\right|^2_{\mathrm{V},\Omega} &= \left|\left|\left| \mathcal{H}\left(\sum_{i=1}^{N_c}(\chi_i u-\chi_i I^0 u)\right)\right|\right|\right|^2_{\mathrm{V},\Omega} \\
&\preceq \sum_{i=1}^{N_c}|||\mathcal{H}(\chi_i u-\chi_i I^0 u)|||^2_{\mathrm{V},\omega_i} \preceq \sum_{i=1}^{N_c}|||\chi_i(u-I^0 u)|||^2_{\mathrm{V},\omega_i},
\end{aligned}$$

where at the last step we have applied Lemma 5.2 on each coarse neighborhood ω_i. Consequently,

$$\begin{aligned}
|||u-u_0|||^2_{\mathrm{V},\Omega} &\preceq \sum_{i=1}^{N_c}|||\chi_i(u-I^0 u)|||^2_{\mathrm{V},\omega_i} + H^2\,\|f\|^2_{L^2(\omega_i)} \\
&\preceq \sum_{i=1}^{N_c}\int_{\omega_i}\chi_i^2|\nabla(u-I^0 u)|^2 + \int_{\omega_i}\kappa^{-1}\chi_i^2|u-I^0 u|^2 \\
&\quad + M\int_{\omega_i}\chi_i^2|\mathrm{div}\,(u-I^0 u)|^2 + M\int_{\omega_i}|\nabla\chi_i|^2|u-I^0 u|^2 + H^2\,\|f\|^2_{L^2(\omega_i)}.
\end{aligned}$$

By applying Lemma 5.5 to the term $u-I^0 u$ in Eq. (25), we deduce

$$\begin{aligned}
|||u-u_0|||^2_{\mathrm{V},\Omega} &\preceq \sum_i M\int_{\omega_i}|\nabla\chi_i|^2|u-I^0 u|^2 + \int_{\omega_i}(\kappa^{-1})^2|u-I^0 u|^2 \\
&\quad + M\int_{\omega_i}\chi_i^2|\mathrm{div}\,(u-I^0 u)|^2 + H^2\,\|f\|^2_{L^2(\omega_i)} + \|p_c\|^2_{L^2(\omega_i)}.
\end{aligned}$$

Finally, using the spectral problem (8), with A and S defined by

$$\begin{aligned}
A &= [a_{mn}] = \int_{\omega_i}(\chi_i)^2\nabla\psi_m^{\omega,\mathrm{snap}}\cdot\nabla\psi_n^{\omega,\mathrm{snap}}, \\
S &= [s_{mn}] = \int_{\omega_i}(\kappa(x)^{-2}+M(\nabla\chi_i)^2)\psi_m^{\omega,\mathrm{snap}}\cdot\psi_n^{\omega,\mathrm{snap}} + M\int_{\omega_i}(\chi_i)^2\mathrm{div}\,\psi_m^{\omega,\mathrm{snap}}\mathrm{div}\,\psi_n^{\omega,\mathrm{snap}},
\end{aligned} \tag{26}$$

we have

$$\int_{\omega_i}M(\nabla\chi_i)^2|u-I^0 u|^2 + \int_{\omega_i}(\kappa^{-1})^2|u-I^0 u|^2 + M\int_{\omega_i}(\chi_i)^2|\mathrm{div}\,(u-I^0 u)|^2 \le \frac{1}{\lambda^{\omega_i}_{L_i+1}}\int_{\omega_i}(\chi_i)^2|\nabla(u-I^0 u)|^2.$$

Hence,

$$|||u-u_0|||^2_{\mathrm{V},\Omega} \preceq \sum_i\frac{1}{\lambda^{\omega_i}_{L_i+1}}\int_{\omega_i}(\chi_i)^2|\nabla(u-I^0 u)|^2 + H^2\,\|f(x)\|^2_{L^2(\omega_i)} + \|p_c\|^2_{L^2(\omega_i)}.$$

Upon denoting $\Lambda_* = \min_{\omega_i}\lambda^{\omega_i}_{L_i+1}$, we deduce

$$|||u-u_0|||^2_{\mathrm{V},\Omega} \preceq \frac{1}{\Lambda_*}\sum_i\int_{\omega_i}(\chi_i)^2|\nabla(u-I^0 u)|^2 + H^2\,\|f(x)\|^2_{L^2(\omega_i)} + \|p_c\|^2_{L^2(\omega_i)}.$$

Using the inequality $\left\|\nabla I^0 u\right\|_{L^2(\omega_i)} \preceq \|\nabla u\|_{L^2(\omega_i)}$,

$$|||u-u_0|||^2_{\mathrm{V},\Omega} \preceq \frac{1}{\Lambda_*}\sum_i\|\nabla u\|^2_{L^2(\omega_i)} + H^2\,\|f(x)\|^2_{L^2(\omega_i)} + \|p_c\|^2_{L^2(\omega_i)},$$

and thus

$$|||u - u_0|||^2_{V,\Omega} \preceq \frac{1}{\Lambda_*} \|\nabla u\|^2_{L^2(\Omega)} + H^2 \|f(x)\|^2_{L^2(\Omega)} + \|p_c\|^2_{L^2(\Omega)}.$$

This completes the proof of the theorem. □

Remark 5.8. We note that in the analysis, we have used the spectral problem (26), instead of (8) in the numerical simulation. In view of the inequality $\|\operatorname{div} u\|_{L^2(D)} \leq \|\nabla u\|_{L^2(D)}$ for any $u \in (H^1(D))^d$ and the fact that χ_i is bounded, these two spectral problems are equivalent provided that M is bounded. Hence our analysis does provide partial justification for the algorithm. The constant M appears as a result of the definition of the velocity and pressure norms, cf. (9) and (10), which is needed for the inf–sup condition. It remains unclear how to get rid of the constant M in the norm definition in the convergence analysis.

6. Conclusion

In this work, we have developed a mixed generalized multiscale finite element method for the Brinkman flow in high-contrast media, which capture both the Stokes flow and the Darcy flow in respective regions. In the fine grid, we approximate the velocity and pressure with piecewise quadratic and piecewise constant functions. We develop a novel approach to construct a coarse approximation for the velocity snapshot space, and a robust low-dimensional offline space for the velocity. The main feature of our approach is to select the important modes by solving certain appropriate local eigenvalue problem. The stability of the mixed GMsFEM and a priori error estimates are derived. The two-dimensional numerical examples illustrate clearly the robustness and efficiency of our method. Besides, it also shows the consistency with the convergence analysis.

In our discussion, we have focused on the approximation of the velocity space, and simply take the piecewise constant space as the approximation space for pressure. This may not be the best choice. The mixed finite element space may get better results with a better pressure space and accordingly an enriched velocity space. Further, it is natural to extend the proposed method to the Stokes model in perforated domains.

Acknowledgment

G. Li's research is partially supported by the U.S. Department of Energy Office of Science, Office of Advanced Scientific Computing Research, Applied Mathematics program under Award Number DE-FG02-13ER26165.

References

[1] A. Gulbransen, V. Hauge, K. Lie, A multiscale mixed finite-element method for vuggy and naturally-fractured reservoirs, NSCM-21.
[2] A.-R. Khaleda, K. Vafai, The role of porous media in modeling flow and heat transfer in biological tissues, Int. J. Heat Mass Transfer 46 (26) (2003) 4989–5003.
[3] O. Iliev, R. Lazarov, J. Willems, Variational multiscale finite element method for flows in highly porous media, Multiscale Model. Simul. 9 (4) (2011) 1350–1372.
[4] P. Popov, G. Qin, L. Bi, Y. Efendiev, R. Ewing, Z. Kang, J. Li, Multiscale methods for modeling fluid flow through naturally fractured carbonate karst reservoirs, in: Proceedings of the SPE Annual Technical Conference and Exhibition, 2007. SPE 110778.
[5] Y. Efendiev, J. Galvis, R. Lazarov, J. Willems, Robust domain decomposition preconditioners for abstract symmetric positive definite bilinear forms, ESAIM Math. Model. Numer. Anal. (2012) 1175–1199.
[6] L. Durlofsky, J.F. Brady, Analysis of the Brinkman equation as a model for flow in porous media, Phys. Fluids 30 (1987) 3329–3341.
[7] F.J. Valdes-Parada, J.A. Ochoa-Tapia, J. Alvarez-Ramirez, On the effective viscosity for the Darcy–Brinkman equation, Physica A 385 (1) (2007) 69–79.
[8] X. Xie, J. Xu, G. Xue, Uniformly-stable finite element methods for Darcy–Stokes–Brinkman models, J. Comput. Math. 26 (2008) 437–455.
[9] D. Brown, Y. Efendiev, G. Li, V. Savatorova, Homogenization of high-contrast Brinkman flows, submitted for publication, 2013.
[10] L. Durlofsky, Numerical calculation of equivalent grid block permeability tensors for heterogeneous porous media, Water Resour. Res. 27 (1991) 699–708.
[11] X. Wu, Y. Efendiev, T. Hou, Analysis of upscaling absolute permeability, Discrete Contin. Dyn. Syst. Ser. B 2 (2002) 158–204.
[12] T. Arbogast, Analysis of a two-scale, locally conservative subgrid upscaling for elliptic problems, SIAM J. Numer. Anal. 42 (2004) 576–598. (electronic).
[13] C.-C. Chu, I.G. Graham, T.-Y. Hou, A new multiscale finite element method for high-contrast elliptic interface problems, Math. Comp. 79 (2010) 1915–1955.
[14] Weinan E, Bjorn Engquist, Heterogeneous multiscale methods, Commun. Math. Sci. 1 (2003) 87–132.
[15] Y. Efendiev, J. Galvis, X. Wu, Multiscale finite element methods for high-contrast problems using local spectral basis functions, J. Comput. Phys. 230 (2011) 937–955.
[16] Y. Efendiev, T. Hou, Multiscale Finite Element Methods: Theory and Applications, in: Surveys and Tutorials in the Applied Mathematical Sciences, vol. 4, Springer, New York, 2009.
[17] Y. Efendiev, T. Hou, V. Ginting, Multiscale finite element methods for nonlinear problems and their applications, Commun. Math. Sci. 2 (2004) 553–589.
[18] E. Chung, Y. Efendiev, R. Gibson, An energy-conserving discontinuous multiscale finite element method for the wave equation in heterogeneous media, Adv. Adapt. Data Anal. 3 (2011) 251–268.
[19] Y. Efendiev, J. Galvis, T. Hou, Generalized multiscale finite element methods, J. Comput. Phys. 251 (2013) 116–135.
[20] M. Ghommem, M. Presho, V.M. Calo, Y. Efendiev, Mode decomposition methods for flows in high-contrast porous media. Global–local approach, J. Comput. Phys., 253, 226–238.
[21] E. Chung, Y. Efendiev, Reduced-contrast approximations for high-contrast multiscale flow problems, Multiscale Model. Simul. 8 (2010) 1128–1153.
[22] E. Chung, W.T. Leung, A sub-grid structure enhanced discontinuous Galerkin method for multiscale diffusion and convection–diffusion problems, Commun. Comput. Phys. 14 (2013) 370–392.
[23] E. Chung, Y. Efendiev, W.T. Leung, Generalized multiscale finite element method for wave propagation in heterogeneous media, 2013. Preprint, Available as arXiv:1307.0123.

[24] B. Muljadi, J. Narski, A. Lozinski, P. Degond, Non-conforming multiscale finite element method for stokes flows in heterogeneous media. Part I: methodologies and numerical experiments, submitted for publication, 2014.
[25] Y. Efendiev, J. Galvis, F. Thomines, A systematic coarse-scale model reduction technique for parameter-dependent flows in highly heterogeneous media and its applications, Multiscale Model. Simul. 10 (2012) 1317–1343.
[26] F. Brezzi, M. Fortin, Mixed and Hybrid Finite Element Methods, Springer-Verlag, Berlin, Heidelberg, New York, 1991.
[27] S. Brenner, L. Scott, The Mathematical Theory of Finite Element Methods, Springer-Verlag, New York, 2007.